AIAA JOURNAL
Vol. 43, No. 11, November 2005

Zonal-Detached-Eddy Simulation of the Flow Around a High-Lift Configuration

Sebastien Deck*
ONERA, 92322 Châtillon Cedex, France

A zonal hybrid Reynolds-averaged Navier–Stokes large-eddy simulation (RANS/LES) approach, called zonal-DES, used to handle a two-dimensional high-lift configuration with deployed slat and flap is presented. This method allows to reduce significantly the cost of an accurate numerical prediction of the unsteady flow around wings compared to a complete LES. Some issues concerning grid generation as well as the use of zonal-detached-eddy simulation for a multi-element airfoil are discussed. The basic planar grid has 250,000 points and the finest spanwise grid has 31 points with $\Delta z/c = 0.002$. The effort is geared toward detailed comparison of the numerical results with the Europiv2 experimental particle image velocimetry data including both mean and fluctuating properties of the velocity field (Arnott, A., Neitzke, K. P., Agocs, J., Sammer, G., Schneider, G., and Schroeder, A., "Detailed Characterisation Using PIV of the Flow Around an Aerofoil in High Lift Configuration," *EUROPIV2 Workshop on Particle Image Velocimetry*, Springer, Berlin, 2003). The results also provide an insight into the real unsteady nature of the flow around a three-element airfoil that cannot be reproduced by classical RANS models. The current calculation displays extremely complex flow dynamics in the slat and flap coves like the ejection process through the gaps of several vortices issued from the impingement of the free shear layers on the lower walls of the different elements.

Introduction

DURING the past few years, the ability to design efficient wings in transonic flight conditions has been mainly influenced by the increased capability and reliability of computational fluid dynamics (CFD) codes in predicting these flows. As a result, wings loading in transonic cruise flight conditions have been enlarged and are now associated with increasing demands on the design of the high-lift system to retain or even increase the same takeoff and landing performance, climb rate, and community noise. (See, for example, discussions in the papers by Woodward and Lean[1] and Thibert et al.[2]) To achieve this goal, a comprehensive understanding of the flow physics is needed to optimize the high-lift systems. Therefore, research activities have been intensified in the last few years including both numerical and experimental efforts.

Indeed, the flow over a multi-element airfoil is inherently complex and exhibits a wide range of physical phenomena including large low-speed areas with the possibility of limited supersonic areas on front elements, strong pressure gradients, unsteady flow regions, three-dimensional effects, and confluence of boundary layers and wakes. Each of the aforementioned topics is a very challenging issue for numerical simulation and needs to be addressed by advanced modeling methods, which are necessary to explore and enhance the performance of the high-lift system. Therefore, Reynolds-averaged Navier–Stokes (RANS) methods have been the focus of most of the past research papers on this topic including two-dimensional[3–5] and three-dimensional steady calculations.[6–8] In particular, stall mechanisms and Reynolds and Mach number effects, as well as sweep effects, have been studied. The three-dimensional steady calculations concerned mainly the analysis of the flap-side edge flowfield,[9–11] flow control device investigations,[12,13] wind-tunnel effects,[14] and complete aircraft configurations.[15] An extensive review of computational capabilities for the simulation of high-lift wing flows was recently conducted by Rumsey and Ying.[16] The authors concluded that an important area of improvement required for the prediction of high-lift system aerodynamics includes unsteady effects. This need is becoming increasingly important because environmental concerns require substantial reductions in noise and emissions.

More precisely, the aerodynamic noise generated by high-lift devices such as slat and flaps of large airliners is an important contributor to the total radiated airframe noise especially in approach and landing configurations. The problem of airframe noise is of outstanding importance due to the huge growth in aircraft noise regulations around airports and the continued efforts in reducing engine noise. This important and pressing issue has lead to the development of computational aeroacoustics which aims at directly resolving the propagation of sound waves all the way toward the far-field receivers. Advanced turbulence modeling simulations can give sufficiently accurate prediction of the near-field flow, which permits reasonably accurate prediction of noise using the acoustic analogy-based methods. To this end, large eddy simulation (LES) offers interesting prospects to simulate the fluctuating pressure field, but a complete LES of a wing with deployed flap and slat is still well beyond the capability of today computers. Hence, there has been considerable interest in RANS/LES approaches concerning unsteady simulations on local elements rather than the complete deployed configuration and especially around the slat. For instance, extensive studies of the unsteady flow in the slat cove area[17,18] and in the vicinity of the blunt trailing edge[19] have been performed by Khorrami et al. thanks to unsteady Reynolds-averaged Navier–Stokes (URANS) calculations. However, they have found it necessary[17] to switch-off the model effects in the slat cove region to restore the rolled-up vortices in the shear layer because the fully turbulent computations were much too diffusive. From this point of view, their calculation can be considered as a zonal RANS/LES approach. Terracol et al.[20] became interested in a local three-dimensional unsteady simulation thanks to a zonal RANS/LES approach based on the nonlinear disturbance equations developed by Labourasse and Sagaut.[21] They observed important differences concerning the mean flowfield in the slat cove between steady computations and zonal RANS/LES. An additional zonal LES-laminar computations has been performed by Ben Khelil[22] on the same geometry as that used by Terracol et al. The LES region is limited to the slat region. Here again, a direct validation of the near-field predictions was not possible due to a lack of experimental data for this high-lift configuration. A more detailed comparison has nevertheless been performed by Roux et al.[23] These authors became interested in the slat cove area flowfield and selected the configuration corresponding to the the experimental setup of the Europiv1 project.[24] Here again, they used a zonal very large-eddy simulation approach based on a k–ϵ renormalization group model

Received 29 March 2005; revision received 6 July 2005; accepted for publication 6 July 2005.

*Research Scientist, Applied Aerodynamics Department, 29, Avenue de la Division Leclerc, B.P. 72; sebastien.deck@onera.fr.

because they modified the model to lower the eddy viscosity in the slat cove area. The main features of the experimental flowfield were recovered by the simulation even if the size of the primary recirculation bubble was slightly overestimated in the simulation. The status of unsteady three-dimensional RANS/LES calculations for high-lift devices is that very few complete configurations have been calculated.[25] To try to get a better understanding of the flowfield, the scope of this paper is limited to a two-dimensional geometry, which was tested experimentally in the Airbus Bremen Low Speed Wind Tunnel.

The objective of the current study is twofold: 1) to assess the capability of a zonal detached-eddy simulation (DES) method to handle a complete high-lift configuration with deployed slat and flap and 2) to carry out detailed comparisons of numerical results with the Europiv2 experimental data.[26]

Numerical Method

General Description

The solver FLU3M code has been developed by ONERA. It solves the Navier–Stokes equations on multiblock structured grids. The computational domain is divided by blocks; each block is composed of structured hexahedral cells. The Navier–Stokes equations are discretized using a second-order accurate upwind finite volume scheme and a cell-centered discretization. The Euler fluxes are discretized by a modified AUSM+(P) upwind scheme, which is fully described in Ref. 27.

Unsteady (global time step) and three-dimensional Navier–Stokes simulations are highly CPU demanding. Explicit schemes are not efficient enough for this purpose, and implicit schemes are required. Time discretization is based on second-order accurate Gear's formulation and has been introduced by Péchier.[28] Moreover, the implicit formulation results in the inversion of a large sparse matrix system. The lower–upper factorization simplifies the inversion of the latter implicit system. Further details concerning the numerical method and implementation of turbulence models may be found in Refs. 29 and 30.

This numerical method is the same as that already used to perform LES of the flow around a two-dimensional wing profile in near-stall conditions,[27] as well as around a low-pressure turbine blade,[31] and has also been successfully used to compute LES of the flow over a cavity at high Reynolds number[32] and to compute zonal-DES of transonic buffet over a supercritical airfoil.[33]

Zonal-DES

New industrial needs in aerodynamics concern, for example, the control of noise as well as the capability to predict dynamic loads so that the simulation of three-dimensional unsteady turbulent flows is required. Traditionally, high-Reynolds-number separated flows have been predicted by solving the URANS equations. This approach can be successfully used in cases where flow is forced to be unsteady because of unsteady boundary conditions (such as body motion) for example, in a flowfield characterized by a large-scale separation between the unsteadiness of the mean field and the turbulent motion. Nevertheless, it seems to be generally accepted that the accurate prediction of massive separation is beyond the capabilities of classical URANS approaches. This comes mainly from the fact that dominant eddies in massively separated flows are highly geometry dependent and have not much in common with the standard eddies of the thin shear flows classical RANS turbulence models are designed to model. As a result, performing Reynolds averaging over the entire spectrum of eddies and trying to include those geometric-sensitive eddies is questionable. To the author's knowledge, URANS does not have a rational theoretical background. As an example, the recent paper of Travin et al.[34] is particularly intriguing. The authors presented a slight modification of the $k-\omega$ model that preserves the RANS logic, for example, the turbulence model is not tuned to the grid spacing. They obtained solutions with LES-like behavior in several flows including homogeneous isotropic turbulence, an airfoil in stall conditions, and a cylinder. These results illustrate the lack of consensus regarding unsteady statistical approaches.

On the other hand, the potential accuracy of LES is generally well acknowledged. In practical engineering problems, the high cost of LES comes from the resolution required in the boundary layers, which dramatically raises the range of scales beyond affordability. For instance, Spalart et al.[35] reported an estimate that, for a wing, LES will have to wait until the year 2045, even assuming that wall modeling has been achieved.

To close the gap between RANS and LES, the development of hybrid RANS/LES approaches has received increasing attention among turbulence modeling researchers, CFD code developers, and industrial CFD engineers.[36–40] The motivation is to combine the best features of the RANS approach with those of the LES ones. Indeed, RANS generally predicts attached flow very well with a low computational cost, whereas LES can predict massively separated flows more accurately. A broader review on strategies in turbulence modeling is given by Spalart in Ref. 41.

Among hybrid strategies, the approach that has probably drawn most attention is the DES, which was proposed by Spalart et al.[35] in 1997. This method has given encouraging results for a wide range of flow exhibiting massive separation[42–46] and has since gone through various stages of refinement. The reader is referred to Spalart[47] and Squires[48] for current status and perspectives in DES.

One of the objective of this study is to assess the capability of a zonal-DES method to simulate the complex flowfield encountered on a high-lift device with deployed slat and flap. In the following paragraphs, a brief review of the standard DES model is first given before explaining the motivations to give zonal features to this model.

The DES model was originally based on the Spalart–Allmaras (SA) RANS model that solves a one-equation turbulence model for the eddy viscosity $\tilde{\nu}$:

$$\frac{\mathrm{D}\tilde{\nu}}{\mathrm{D}t} = \underbrace{c_{b1}\tilde{S}\tilde{\nu}}_{\text{production}} + \underbrace{\frac{1}{\sigma}\left(\nabla.(\nu+\tilde{\nu})\nabla\tilde{\nu} + c_{b2}(\nabla\tilde{\nu})^2\right)}_{\text{diffusion}} - \underbrace{c_{w1}f_w\left(\frac{\tilde{\nu}}{d}\right)^2}_{\text{destruction}} \tag{1}$$

The eddy viscosity is defined as

$$\mu_t = \rho\tilde{\nu}f_{v1} = \rho\nu_t, \qquad f_{v1} = \chi^3\Big/\left(\chi^3 + c_{v1}^3\right), \qquad \chi = \tilde{\nu}/\nu \tag{2}$$

To ensure that $\tilde{\nu}$ equals $\kappa y u_\tau$ in the log layer, in the buffer layer, and viscous sublayer, a damping function f_{v1} is defined as

$$f_{v1} = \chi^3\Big/\left(\chi^3 + c_{v1}^3\right) \tag{3}$$

with $\chi = \tilde{\nu}/\nu$. The vorticity magnitude S is modified such that $\tilde{S}$ maintains its log-layer behavior, $\tilde{S} = u_\tau/\kappa y$:

$$\tilde{S} = \sqrt{2\Omega_{ij}\Omega_{ij}} + \frac{\tilde{\nu}}{\kappa^2 d^2}f_{v2}, \qquad \Omega_{ij} = \frac{1}{2}\left(\frac{\partial\tilde{u}_i}{\partial x_j} - \frac{\partial\tilde{u}_j}{\partial x_i}\right) \tag{4}$$

which is accomplished with the help of the functions

$$f_{v2} = 1 - \chi/(1+\chi f_{v1}) \tag{5}$$

To obtain faster decaying behavior of the destruction in the outer region of the boundary layer, a function f_w is used:

$$f_w(g) = g\left[\frac{\left(1+c_{w3}^6\right)}{\left(g^6+c_{w3}^6\right)}\right]^{\frac{1}{6}}$$

$$g = r + c_{w2}(r^6 - r), \qquad r = \frac{\tilde{\nu}}{\tilde{S}\kappa^2 d^2} \tag{6}$$

where g acts as a limiter that prevents large values of f_w. Both r and f_w are equal to 1 in the log layer and decrease in the outer region. Constants of the model are

$$c_{b1} = 0.1355, \qquad c_{b2} = 0.622, \qquad \sigma = \tfrac{2}{3}, \qquad \kappa = 0.41$$

$$c_{w1} = c_{b1}/\kappa^2 + (1+c_{b2})/\sigma, \qquad c_{w2} = 0.3$$

$$c_{w3} = 2, \qquad c_{v1} = 7.1 \tag{7}$$

For the current research, the transition terms were turned off, and we refer to the original papers[49,50] for further details on the constants and the quantities involved.

What is important here is that the model is provided with a destruction term for the eddy viscosity that contains d, the distance to the closest wall. This term when balanced with the production term, adjusts the eddy viscosity to scale with local deformation rate $\tilde{S}$ producing an eddy viscosity given by

$$\tilde{\nu} \sim \tilde{S} d^2 \tag{8}$$

Following these arguments, Spalart et al.[35] suggested to replace d with a new length $\tilde{d}$ given by

$$\tilde{d} = \min(d, C_{\mathrm{DES}}\Delta) \tag{9}$$

where $\Delta = \max(\Delta_x, \Delta_y, \Delta_z)$ is the computational mesh size. The use of the maximum grid extension is physically justified because it controls which wavelengths can be resolved and the eddy-viscosity level. More precisely, in the attached boundary layer, due to the significant grid anisotropy ($\Delta_x \approx \Delta_z \gg \Delta_y$) typical of this flow region, in accordance with Eq. (9), $\tilde{d} = d$, and the model reduces to the standard SA RANS model. Otherwise, once a field point is far enough from walls ($d > C_{\mathrm{DES}}\Delta$), the length scale of the model performs as a subgrid-scale version of the SA model.

Although encouraging results were obtained over a wide range of configurations, weaknesses of DES were discovered. Especially, the gray zone in which the model needs to convert from fully modeled turbulence (attached boundary layer) to mostly resolved turbulence (massive separation) was recognized as potentially delicate. This situation happens when the switching to LES mode occurs inside the boundary layer, for example, when the grid brings the $\tilde{d} = C_{\mathrm{DES}}\Delta$ branch of Eq. (9) to intrude the boundary layer. The result is a weakened eddy viscosity, but not weak enough to allow LES eddies to form, which yields lower Reynolds stress levels compared to those provided by the RANS model. Note that this issue was already addressed in the original paper presenting the method by Spalart et al.[35] As a result, the separation lines moves too far forward leading to a "Grid-Induced-Separation (GIS)."[38] The region corresponding to $d \approx \Delta$ is called "grey-zone" of DES[35,51] because it is not clear what exactly happens in this region. For example, Nikitin et al.[52] used DES as a wall-layer model in calculations of plane channel flow with different grids exploring a wide range of Reynolds number ($180 \leq Re_\tau \leq 8000$). Their calculations showed some promising results because the turbulence in the outer layer was sustained even in the grid areas not particularly refined [$(\Delta_x^+)_{\max} \approx 8000$]. Nevertheless, the skin-friction coefficient was underpredicted by approximately 15% in most cases. More recently, Piomelli et al.[53] studied more deeply this intermediate blending region within the DES approach. They performed LES of the flow in a plane channel at high Reynolds number by varying the location and extent of this blending layer. Their study shows that the DES buffer layer is characterized by very long eddies, with unphysical long timescales. Improvements were obtained by reducing the value of C_{DES} to bring the outer-flow eddies closer to the wall.

Efforts have been done to try to overcome the GIS drawback but with moderate success. Notice from Eq. (9) that the location of the gray area depends both on the definition of the DES length scale and on C_{DES}. To keep the original value $C_{\mathrm{DES}} = 0.65$ calibrated on isotropic turbulence, Caruelle and Ducros[54] introduced a second constant C_{DES2} only used for selecting the switch position so that $\tilde{d} = C_{\mathrm{DES}}\Delta$ only if $d > C_{\mathrm{DES2}}\Delta$. The modified distance $\tilde{d}$ is, therefore, discontinuous. This approach is, nevertheless, difficult to use in an predictive industrial context. An alternate proposal has been suggested by Forsythe et al.[55] based on a function of d and $C_{\mathrm{DES}}\Delta$ that overshoots $C_{\mathrm{DES}}\Delta$ when they are nearly equal. More precisely, the authors modified the DES length scale according to the equation $\tilde{d} = \min\{C_{\mathrm{DES}} \max[n^2(\Delta/d)C_{\mathrm{DES}}\Delta, \Delta], d\}$ where n is the ratio of the new RANS/LES interface height to the original height. In other words, the parameter n indicates by how much $\tilde{d}$ is allowed to exceed $C_{\mathrm{DES}}\Delta$. The authors used the value $n = 3$ to push the gray area outside of the boundary layer. These proposals have to be viewed as a partial solution because further refinement will defeat them. The gray area needs careful monitoring, but novel approaches are emerging.[38,47,56]

For complex geometries, the design of the DES grid appears to be a dilemma for the user. On one hand, the RANS part of the simulation requires a near-wall grid spacing in the tangential direction that is larger than the boundary-layer thickness at that location to avoid GIS. On the other hand, there is no reason why a DES calculation should accept a coarser grid than an LES calculation. Especially, an LES grid is locally refined in all directions because strongly anisotropic grids are inefficient.[57] As a result, the grid is also refined in regions not intended to be handled by LES. This situation is practically unavoidable in structured grids where refinement is required in some region of high geometric curvature or in the presence of thick boundary layers. Note that both features are encountered on a high-lift device.

This dilemma has motivated the development of the zonal-DES approach,[58] where fully attached boundary-layer regions are treated in RANS mode regardless of the grid resolution. That means that, following the example of RANS/LES coupling methods, the user has to define the RANS and LES zones. The interest of this approach is that the user can focus grid refinement on regions of interest only, for example, LES regions, without corrupting the boundary-layer properties farther upstream or downstream. In addition, the use of special gridding strategies such as patching methods is straightforward. This explicit character of the splitting of the flow zones differs from other RANS/LES coupling because no turbulent fluctuations are reconstructed at the interface[22,59–61] between RANS and LES in the present work. As a consequence, the zonal-DES approach is well adapted to handle separated flows in which strong instabilities are rapidly developing, thus overwhelming the turbulence inherited from upstream boundary layers.

The computational grid has then to be carefully designed. For example, in the LES region, for example, outside boundary layers, the grid is designed to obtain nearly cubic grid cells to use the cube root $\Delta = (\Delta_x \Delta_y \Delta_z)^{1/3}$ as filter-width for LES. This simple modification decreases drastically the level of predicted eddy viscosity because this latter value is proportional to the square of the filter width Δ. We also made the choice to remove the near-wall functions in LES mode formulation (also see Breuer et al.[62]):

$$f_{v1} = 1, \qquad f_{v2} = 0, \qquad f_w = 1 \tag{10}$$

This choice also avoids that the damping functions of the RANS model interpret the low-eddy-viscosity levels typical of resolved LES regions as closeness to the wall with corresponding fast nonlinear drop of subgrid viscosity. (See Guénot[63] for a comparison of several DES implementations.) An alternative proposal that prevents activation of the low Reynolds terms in LES mode has been made by Shur et al.[64] by introducing a threshold function based on the ratio ν_t/ν.

Europiv2 High-Lift Tests

This study concerns a three-element airfoil that was tested in the Low Speed Wind Tunnel of Airbus Bremen (Germany) within the framework of the EUROPIV2 Project G4RD-CT-2000-00190 and used as a test case in the DESider European Project AST-CT-2003-502842. The experimental results presented here were reported by Arnott et al.[26] (See also Neitzke.[65]) Descriptions of the experimental apparatus and procedures are described in those publications. One of the goal of this experimental study was to investigate the flow over slat/wing/flap model in high-lift configuration.

The model is based on an RA16SC1 two-dimensional profile whose geometry is given Fig. 1. The slat and flap angles were set at one position with deflection angles of 30 and 40 deg, respectively. The reference chord is equal to $c = 0.5$ m. The tests were performed using a wind-tunnel freestream speed of $U_\infty = 54\ \mathrm{m \cdot s^{-1}}$ in atmospheric conditions. The Reynolds number based on freestream velocity and the chord length of the main wing is equal to 1.7×10^6.

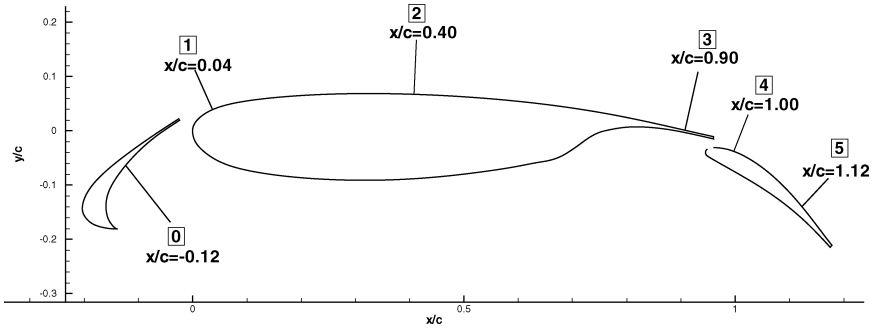

Fig. 1 RA16SC1 model and rake locations.

Data obtained from these investigations consisted of static pressure distribution and a full set of particle image velocimetry (PIV) data. The PIV tests were grouped into four camera arrangements to investigate the flowfield around the high-lift element. In this work, all streamwise location references will be made using the unstowed coordinates and abscissas are normalized by the chord length of the main wing.

Results and Discussion

Grids

Following the example of LES, the grid generation constitutes an important issue in DES because the grid extension controls which wavelengths can be resolved as well as the eddy-viscosity level. As often encountered with complex three-dimensional unsteady computations, our grid design has followed an evolutionary path thanks to initial RANS calculations. The focus regions in the present study are the slat and flap coves, as well as the wake downstream of the main element.

A well-designed grid topology allows one to minimize the number of total grid points while achieving the proper mesh distribution and maintaining the desired level of accuracy in the focus regions. Therefore, the structured multiblock mesh is based on a C–O–H-type topology. The basic two-dimensional grid in the $(x–y)$ plane is divided into 15 blocks leading to a total number of 250,000 nodes. The far-field conditions are imposed at 20–30 times the chord length away from the profile. Furthermore, the resolution of boundary layers is of primary importance for high-lift flow computation. The first point off a wall has y^+ of less then 2 (at worst).

The design of a DES grid around a two-dimensional airfoil requires the specification of two main grid parameters. The first one is the grid extension Δ_z in the spanwise direction, and the second one concerns the global span size of the computational domain $L_z = N_z \times \Delta_z$, where N_z is the number of planes in the spanwise direction. To evaluate the effect of grid refinement, two three-dimensional grids have been built by duplicating the two-dimensional grids in the spanwise direction. The grid extension Δ_z is chosen constant (e.g., uniformly distributed in the homogeneous direction) to have $\Delta_x \approx \Delta_z$ in the "LES-region" following Spalart's recommendations.[57] The retained values are, respectively, $100 \cdot \Delta_z/c = 0.2$ for grid 1 and $100 \cdot \Delta_z/c = 0.3$ for grid 2. Figure 2 presents grid details in the vicinity of the slat cove as well as over the flap.

The spanwise grid can then be obtained by simple duplication of the basic grid. Therefore, the mesh size can become prohibitive because this dense resolution must be kept in the far field and in the wake with a structured solver. In the framework of the LESFOIL project, Mary and Sagaut[27] (also see Ref. 31) developed a two/three-dimensional coupling method to optimize the cell distribution. The main idea is related to the specificity of external flows around an infinite span body which consists in the existence of a large zone where the flow is two dimensional. Indeed, three-dimensional computations can be limited to a zone close to the airfoil where the flow is turbulent, whereas two-dimensional simulations are performed in the far field (except in the wake). This strategy does not affect the accuracy of the simulation as long as the two/three-dimensional

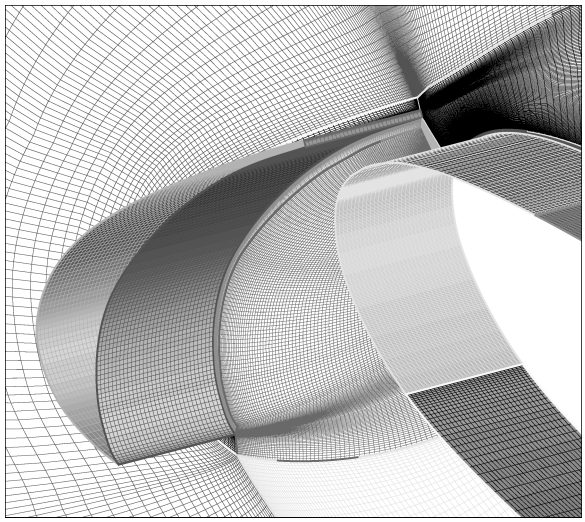

a) Slat

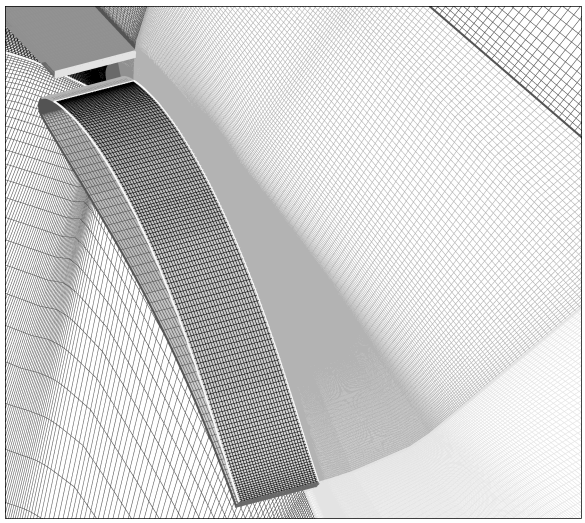

b) Flap

Fig. 2 Grid details (grid 1).

interface is located in regions where the flow is two dimensional. Hence, the zonal topology used for the present DES computations is presented Fig. 3, which shows the two- and three-dimensional domains. This strategy allows to save 2×10^6 nodes leading to a total number of $N_{xyz} = 5.5 \times 10^6$ nodes (instead of $N_{xyz} = 7.5 \times 10^6$). In addition, the normalized spanwise width of the grid is equal to $100 \cdot L_z/c = 6$ for grid 1 and $100 \cdot L_z/c = 9$ for grid 2. Paterson and Peltier[66] (also see Ref. 67) also used a spanwise variation of grid resolution in RANS and DES regions, whereas Khorrami et al.[68] used nonconforming zonal interfaces in the basic two-dimensional grid.

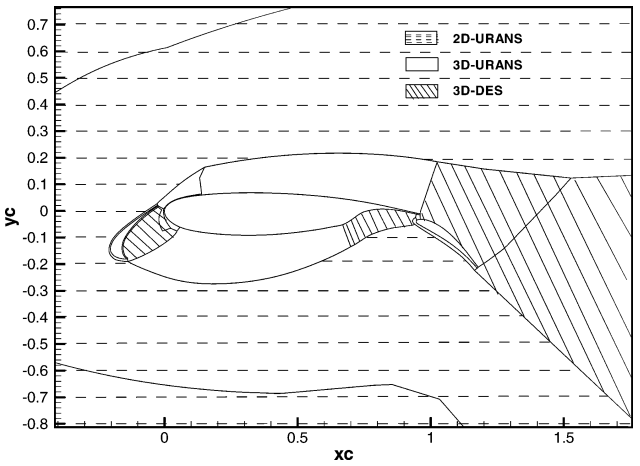

Fig. 3 Grid topology and zonal-DES.

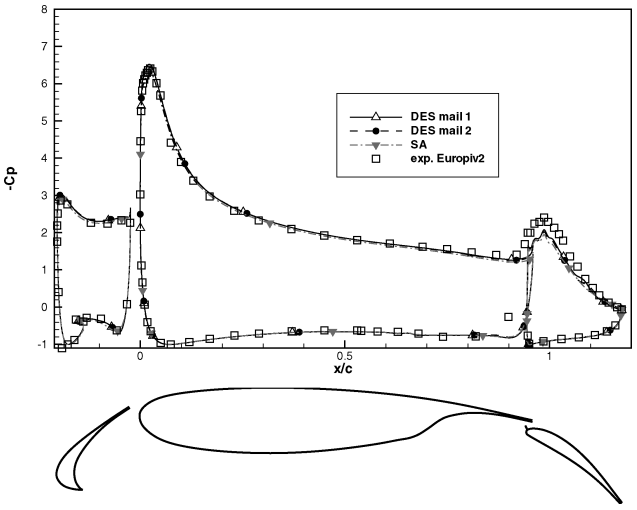

Fig. 4 Pressure coefficient around the airfoil.

Computational Description

For high-lift devices (HLD) computations, the capture of the slat wake and its downstream evolution is of primary importance. The key role played on the $CL_{\max}$ evolutions by the merging of the slat wake with the main body boundary layer was pointed out by several authors, and a good estimation of this phenomenon by the numerical methods is of primary importance.[69–71] Surprisingly, this aspect only received little attention in the literature of RANS/LES computations, which mainly focused on the slat area.

The computation of this wake in LES mode, as well as its evolution downstream of the slat trailing edge, would require extremely fine grids and significant mesh clustering all along the upper side of the main element. In addition, the mixing of this wake with the boundary layer of the main element would dramatically raise the range of scales, and correlatively the CPU cost, beyond affordability. Therefore, the focus regions in the current study are limited to the slat and flap coves, as well as to the flowfield over the flap. The mixing of the slat wake with the boundary layer is explicitely treated in RANS mode as shown Fig. 3. Note that the zonal approach based on physical arguments was advocated and pursued by Khorrami et al.[17] These authors argued that the energy-containing, large-scale coherent structures in the cove region are predominantly responsible for the far-field noise.

Although, a significant portion of the flow over the slat upper surface may have been laminar, in practice because no transition was set in the experiment,[1] all of the present computations were performed assuming fully turbulent boundary layers over all three elements. For more discussion on transitional effect issues on high-lift configurations, see for example Refs. 5 and 72. The computations and postprocessing of the results are based on nondimensionalized flow quantities. The average procedure is performed both in time and in the homogeneous spanwise direction during the calculation. Zonal-DES calculations are carried out in three steps. First a RANS calculation provides an initial flow solution. After the transient phase, the real unsteady calculation to collect statistics begins.

The CPU cost per cell and per inner iteration is less than 1 μs. The simulations are performed on a single processor of an NEC-SX6 supercomputer, and the code is running approximatively at 4×10^9 floating-point operations per second. The time step is fixed to $\Delta t_{\mathrm{CFD}} = 0.2$ μs, for example, $\Delta\tilde{t} = \Delta t_{\mathrm{CFD}} U_\infty / c = 2.2 \times 10^{-5}$ with four Newton inner iterations yielding a maximum Courant–Friedrichs–Lewy number based on acoustic velocity $(U + a)$ equal to 4 located in the attached boundary layers.

The presence of tunnel walls does affect the recirculation and, thus, loading on the leading-edge slat. To match the mean slat loading, the way we use the CFD calculation is an adaptation of the angle of attack to the suction peak at the main wing and slat. This adaptation is performed thanks to preliminary RANS calculations. Results presented in this paper were obtained with a 9-deg angle of attack (compared to 12 deg for the experiment), which was found to yield the best match with the pressure distribution on the main wing. This methodology has also been used by Khorrami et al.[19] and is commonly used for HLD calculations.

Therefore, in Fig. 4 a comparison to the experiment of the averaged pressure coefficient on each element is shown. First notice that, at this angle of attack, the main element carries the highest loads. Both RANS and zonal-DES compare favorably with experiment except on the flap. Indeed, the suction peak on the flap is not well reproduced by calculations. The presence of laminar bubbles, which are usually associated with high peak suction and steep adverse pressure gradient, is not taken into account. The flowfield over the flap will be investigated next.

Flow over the Slat

Instantaneous Flowfield

It is desirable to study the slat flow first because its effect is convected all of the way downstream. The flowfield over the slat is not well understood and is difficult to predict.

The turbulent structures are exhibited showing a positive isovalue of the criterion $\mathcal{Q}$ (Ref. 73). It defines as vortex tubes the regions where the second invariant of velocity gradient tensor $\mathcal{Q}$ is positive:

$$\mathcal{Q} = \frac{1}{2}(\Omega_{ij}\Omega_{ij} - S_{ij}S_{ij}) = -\frac{1}{2}\frac{\partial u_i}{\partial x_j}\frac{\partial u_j}{\partial x_i} > 0 \qquad (11)$$

where S_{ij} and Ω_{ij} are the symmetric and antisymmetric components of ∇u, respectively.

Figure 5 shows a positive value of the Q criterion colored by the transvere velocity component. Figure 5 clearly illustrates the rollup of two-dimensional eddies in the free shear layer that progressively become three dimensional when they impact the lower side of the slat. More precisely, after experiencing severe distorsion at the reattachment point, some large and strong vortex are entrapped in the cove. The coherent vortical structures in the shear layer have also been observed in PIV results of Takeda et al.[74] In addition, Fig. 5 shows a snapshot of the Q criterion in the vicinity of the slat trailing edge and shows the ejection process through the gap of several vortices, but there is no direct impingement of these eddies on the leading edge of the main element. These observations corroborate the PIV measurements of different teams in North America[75,76] and in Europe.[1,74]

Let us recall that zonal-DES relies on a single set of model equations and a continous treatment at the RANS/LES interface. The decrease of eddy viscosity farther away from solid walls allows three-dimensional eddies to develop rapidly (like Kelvin-Helmoltz instability in low-convective Mach number free shear layers) but no turbulent fluctuations are explicitly reconstructed at the RANS/LES interface. These eddies are then advected through the gap and affect the flow over the main wing as discussed later.

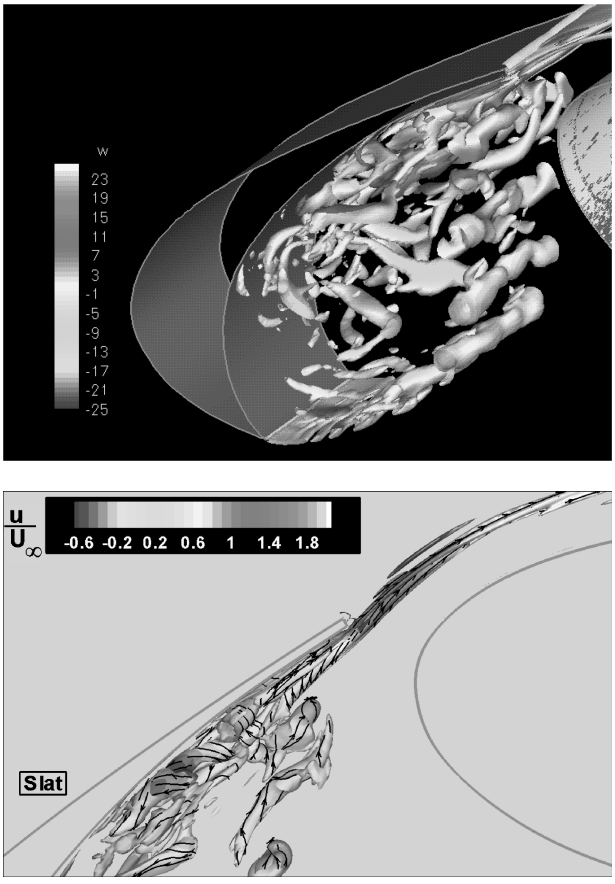

Fig. 5 Description of the instantaneous flowfield in the slat area (zonal-DES grid 1).

Averaged Flowfield

Computed and experimentally statistical-averaged velocity magnitude are compared to the experiment in Fig. 6. The time-averaged velocity magnitude contours near the leading-edge slat clearly displays the acceleration of the local flow through the gap as well as the recirculation zone. This low-speed recirculation area on the suction side of the slat is bounded by the mixing layer that develops in the shear layer. The flow acceleration through the slat/wing gap is particularly prominent. The development of the slat wake and gap flow is also evidenced. It is observed that the mean velocity fields obtained by zonal-DES are in fair agreement with experiment, showing that the dynamics in the slat cove is accurately predicted. One can notice only small differences between RANS and zonal-DES in the vicinity of the slat wake.

Figure 7 then shows a comparison to experiment of the predicted streamlines around the slat and clearly shows the large separation on the lower surface of the slat and the point of reattachment. The flow is attached at the upper surface trailing edge of both the main airfoil and the flap. In addition, the size of the separation is well reproduced for both RANS and zonal-DES.

To get a more detailed comparison of numerical results with experimental data, Fig. 8 shows the velocity profile for a rake located in the slat cove. The rake locations are given Fig. 1. The streamwise coordinates in percent chord of the main wing are also given. Experimental profiles are extracted from PIV maps. Note also that, in Fig. 8 and subsequently, d/c refers to the local wall-normal distance normalized by the reference length. All velocity profiles presented are velocity magnitudes normalized by the freestream velocity.

This profile (rake 0) shows a significant velocity gradient between the cove and the outer flow. Notice that the center of the recirculation bubble located near $d/c \approx 0.04$ (defined by $U \approx 0$) is well reproduced for both RANS and zonal-DES. The boundary of the shear layer near $d/c \approx 0.1$ (defined by the maximum of U) is also well located, especially by the zonal-DES calculations. Only some

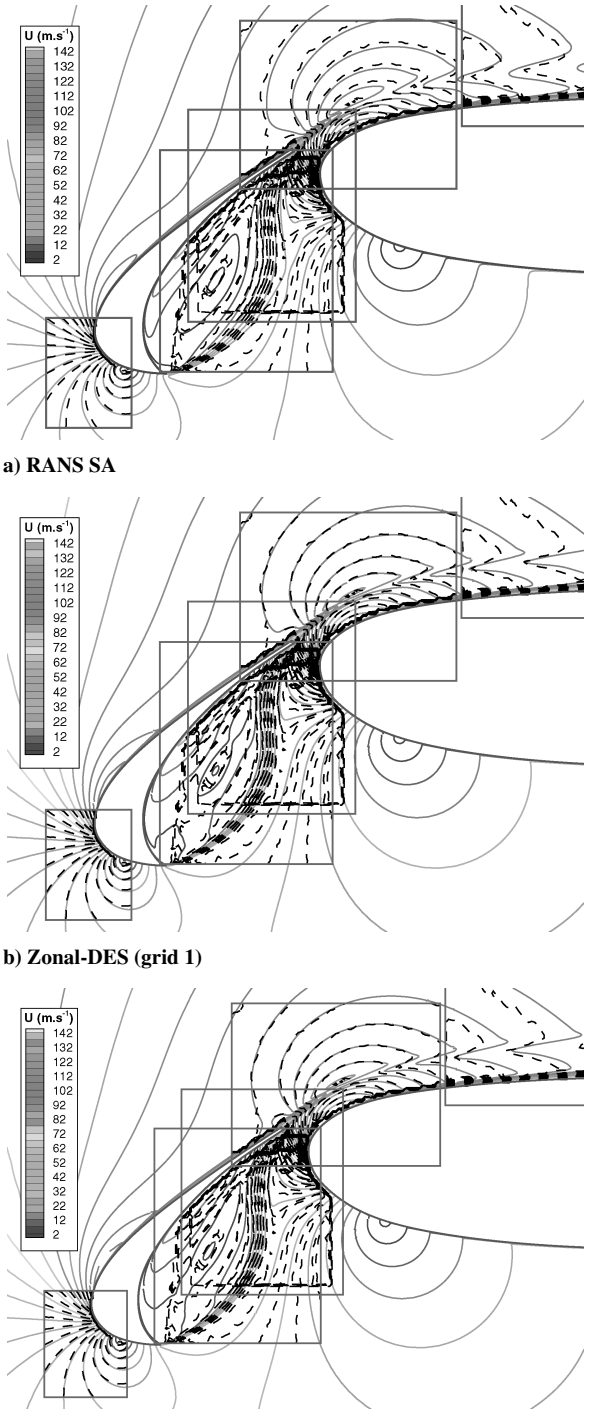

a) RANS SA

b) Zonal-DES (grid 1)

c) Zonal-DES (grid 2)

Fig. 6 Comparison of magnitude of velocity in slat area: - - - -, experimental and ——, computed.

minor differences concerning the velocity inside the trapped bubble are depicted.

The velocity component fluctuations profiles are then plotted in Fig. 9. Indeed, the flow in the slat cove is unsteady because the path of the shear layer wanders both in time and space. Figure 9a shows a comparison to the experiment of the rms fluctuation of the steamwise component of velocity. These levels remain nearly constant at $u_{\text{rms}}/U_\infty \approx 6\%$ within the bubble. Twice as high rms levels are encountered for the vertical velocity component (Fig. 9b). Minor differences are observed between the two grids.

Of interest is the level of fluctuations of tranverse velocity component (Fig. 9c). The highest levels, $w_{\text{rms}}/U_\infty \approx 9\%$, are obtained in the vicinity of the slat lower surface. This result can be interpreted

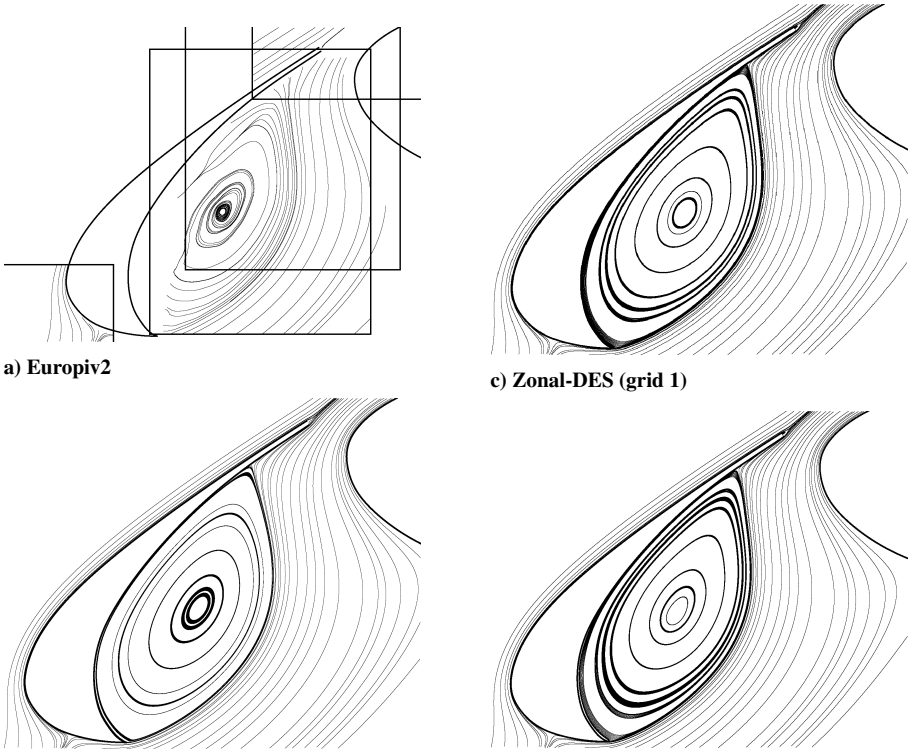

a) Europiv2

c) Zonal-DES (grid 1)

b) SA

d) Zonal-DES (grid 2)

Fig. 7 Averaged streamlines in the slat cove area.

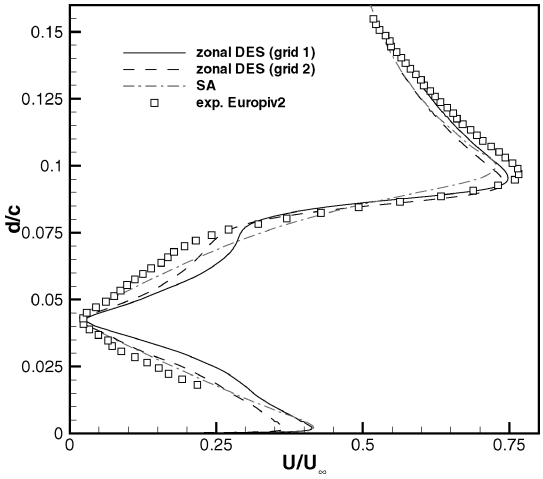

Fig. 8 Velocity profiles, rake 0.

in connection with Fig. 5. Indeed, this Fig. 9c shows the highly three-dimensional flow structures in the slat cove where the flow reverses.

The turbulent kinetic energy k_{uv} was estimated using two components of the fluctuating flowfield, although this is not equivalent to the true kinetic energy (TKE). Notice the experimental nonzero turbulence level outside of the bubble compared to the calculation. The highest levels are obtained in the shear layer at $d/c \approx 0.04$. The calculations underestimate this level because $(\sqrt{k_{uv}}/U_\infty)_{\max} \approx 10\%$ for the calculation, whereas $(\sqrt{k_{uv}}/U_\infty)_{\max} \approx 12\%$ for the experiment. Such levels of fluctuation highlight the unsteady behavior of the flow and not only the turbulence itself. However, the freestream turbulence level cannot be reproduced by the SA turbulence model without further additional modeling assumptions. The level of TKE remains important in the whole recirculation bubble, whereas from the numerical side, the level of fluctuations decreases in the bubble to reach a minimum $(\sqrt{k_{uv}}/U_\infty)_{\min} \approx 6\%$ before increasing again in the vicinity of the lower surface. This last increase is due to the reattachment process, which produces large velocity fluctuations. These numerical results corroborates recent findings of Jenkins et al.[76] These authors reported PIV images of TKE inside the bubble of the 30P30N airfoil. They observed that the highest levels are located in the shear layer and in the vicinity of the lower surface near the reattachment, but much lower levels were obtained between these two boundaries. Indeed these authors obtained $\sqrt{\text{TKE}}/U_\infty \approx 7\%$ in the center of the bubble.

Flow over the Main Element

Upper Side

Computed and experimentally statistical-averaged velocity magnitude around the main wing are compared to experiment in Fig. 10. The time-averaged velocity magnitude contours near the leading-edge flap displays the acceleration of the local flow through the gap, as well as the recirculation zone. Important stages such as merging of the slat wake and the main element boundary layer are shown. Notice that the spreading of the separating shear layer from the flap cove lip is more pronounced with the RANS computation than with zonal-DES.

Figure 11a allows one to compare the flow acceleration through the slat/wing gap to the experiment. The computed slat–wake width and deficit is evidenced. The flow scale at the trailing edge is so small that the accuracy of the measurements is affected by the spatial resolution of the PIV window. Arnott et al.[26] indicate that the accuracy ϵ/c in the $(x–y)$ coordinates of the vectors is 10^{-3}. The height of the slat blunted trailing edge is equal to $h/c = 3 \times 10^{-3}$. RANS and zonal-DES are both in good agreement with the experiment, only small variations being observed on the flow maximum acceleration through the gap.

The merging between the slat wake and the main wing boundary layer is evidenced in Fig. 11b. Recall that this merging is in most cases the driving phenomenon for the maximum lift coefficient. Therefore, the zonal-DES approach allows one to model the physics of the mean flow and, in addition, to access the characteristics of the fluctuating flowfield.

Figure 11c then shows the velocity profile at the main wing trailing edge (rake 3). The agreement of the slat wake and merging

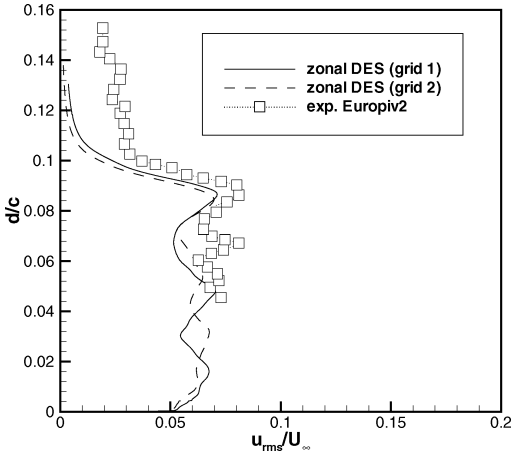

a) $u_{\mathrm{rms}}/U_\infty$

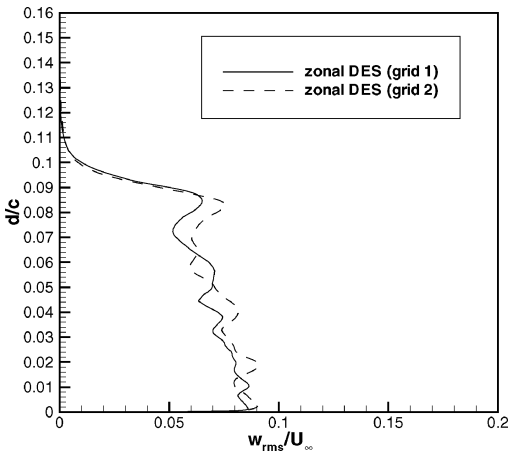

c) $w_{\mathrm{rms}}/U_\infty$

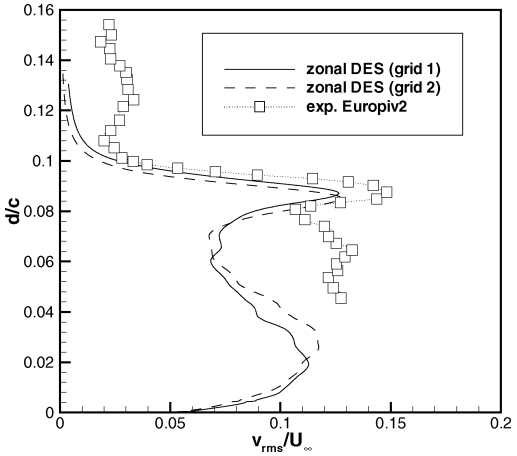

b) $v_{\mathrm{rms}}/U_\infty$

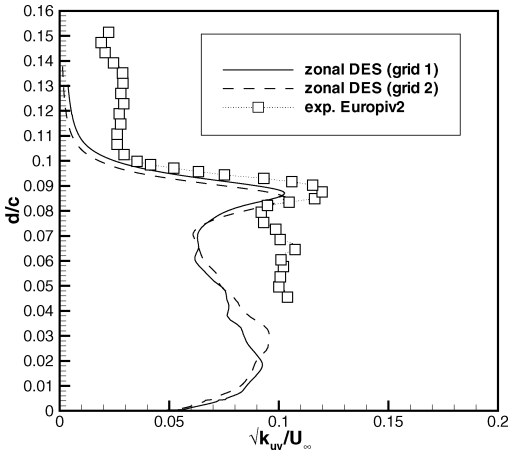

d) $\sqrt{k_{uv}}/U_\infty$

Fig. 9 Velocity fluctuations profiles, rake 0.

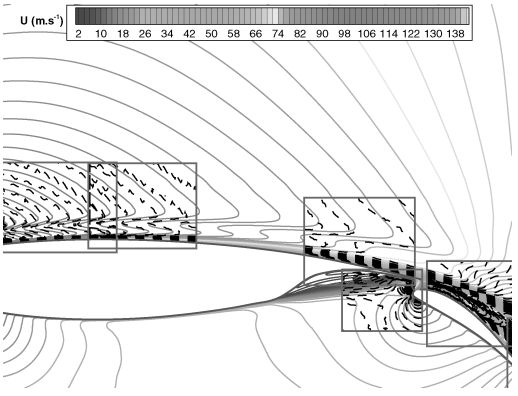

a) RANS SA

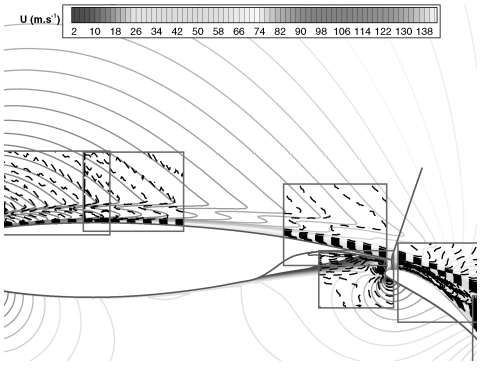

b) Zonal-DES (grid 1)

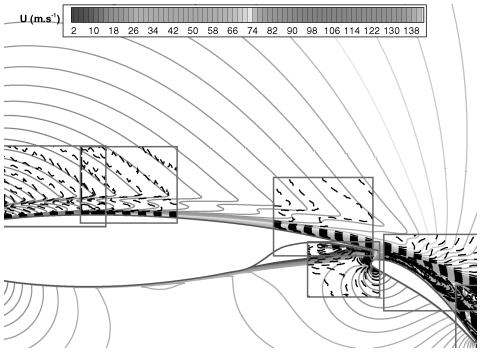

c) Zonal-DES (grid 2)

Fig. 10 Comparison of magnitude of velocity on wing: - - - -, experimental and ——, computed.

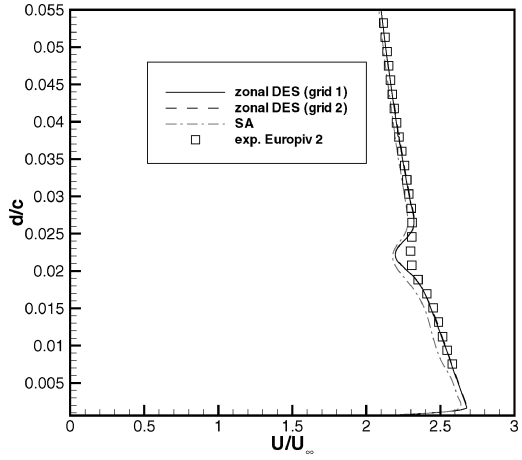

a) Rake 1

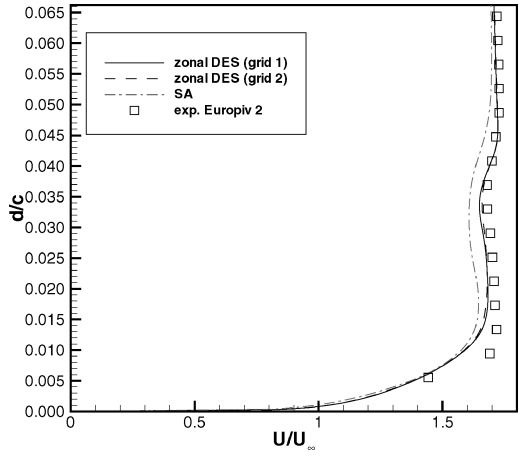

b) Rake 2

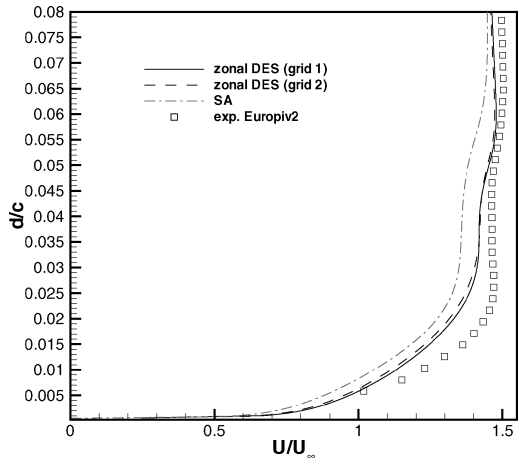

c) Rake 3

Fig. 11 Velocity profiles on wing: ----, experimental and ——, computed.

region for the RANS calculation is much poorer because the layer adjacent to the wall shows an underestimation of the velocity magnitude compared to experiment. This is certainly because the present calculations do not take into account the boundary-layer development along the wind-tunnel sidewalls. The better agreement with experiment of the zonal-DES calculation is likely because the calculation takes into account the unsteady flow originating from the slat (Fig. 5) because the upper side of the main element is treated in URANS mode. This result is in accordance with Fig. 4 showing that computations present an underestimation of the peak velocity at the flap leading edge, which induces an underestimation of the flow velocity at the leading edge. Theses differences may also be

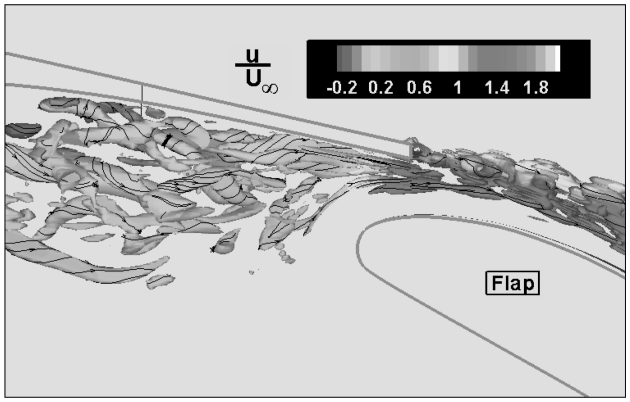

Fig. 12 One isosurface of Q criterion colored by u-component velocity.

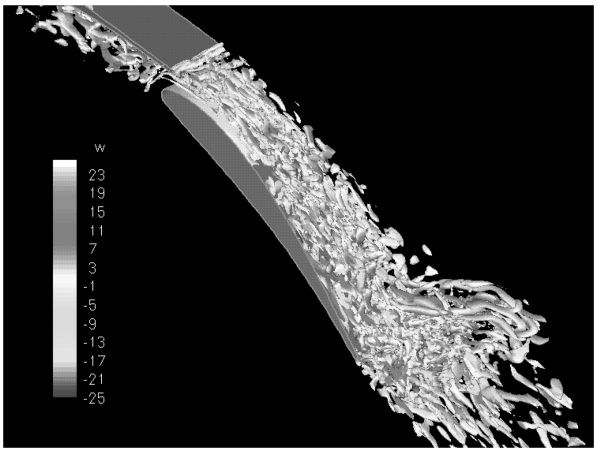

Fig. 13 Isosurface of Q criterion colored by transversal velocity (zonal-DES grid 1).

linked to the possible transitions on upstream elements that are not taken into account. In other words, the boundary layer that leaves the slat or on the wing is probably too thick in the calculation. Indeed, Rumsey et al.[4] introduced a subset of transition locations for a two-dimensional three-element airfoil configuration to demonstrate the importance of accurately modeling the transition process. They used three turbulence models, SA, $k-\omega$ shear stress transport and $k-\omega$ explicit algebraic Reynolds stress model (EARSM), which yielded very similar results. The authors concluded that the poor wake predictions cannot be attributed only to the turbulence model but also have to be attributed in part to deficiencies in transition prediction on the generating element.

Flap Cove

The flap cove flow has many similar features to the leading-edge slat flow, and the current computation displays extremely complex flow dynamics in the flap cove. Figure 12 shows the separating shear layer from the flap cove lip that rapidly becomes unstable, rolls up into large coherent vortices, and impinges the flap cove wall. Figure 12 reveals the three-dimensional unsteady nature of the flow inside the flap cove. The vortices that do escape through the gap are severely deformed and stretched by the accelerating local flow so that they become mainly longitudinal eddies. These observations corroborate the PIV measurements of other experimental teams (see Takeda et al.[77]). Therefore, the flow in the flap cove can influence the flow through the wing/flap gap, which in turn may affect the flow over the flap. The small-scale vortex shedding occurring at the trailing edge of the main element can also be seen.

Flow over the Flap

Instantaneous and Averaged Flowfield

The turbulent structures in Fig. 13 shows the merging and turning effects of the wakes. Important stages such as rollup and formation of discrete vortices can be detected. For example, at the main element

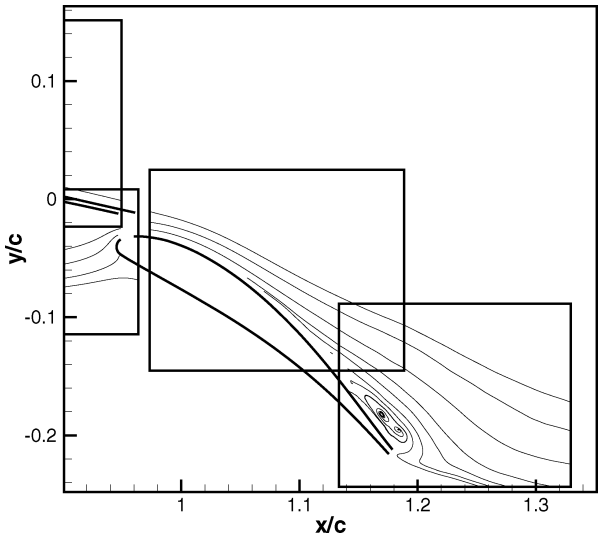

a) Europiv2

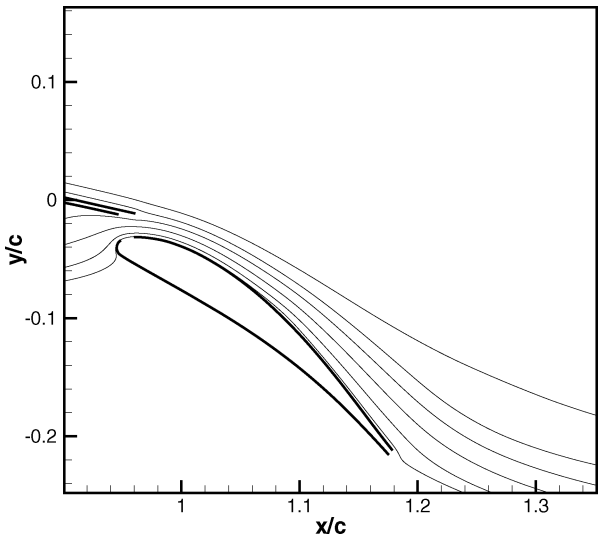

b) Zonal-DES (grid 1)

Fig. 14 Averaged streamlines over the flap.

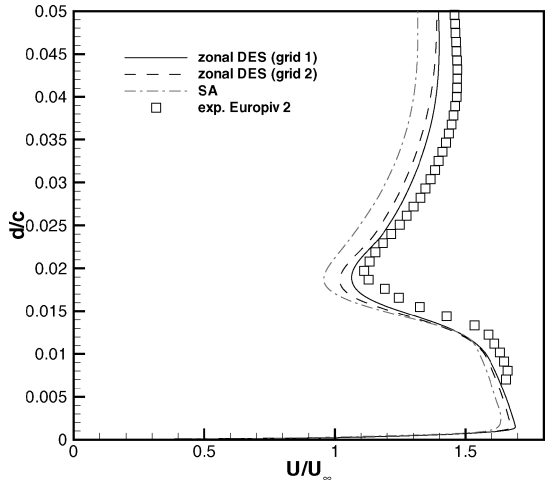

a) Rake 4

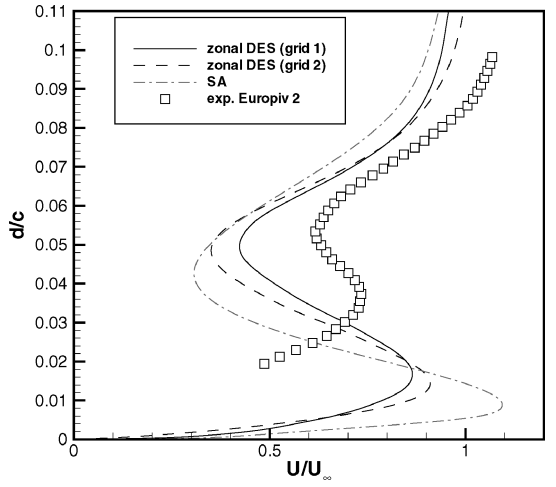

b) Rake 5

Fig. 15 Comparison of magnitude of velocity on flap: - - - -, experimental and ——, computed.

trailing edge, a shear layer evolves, that rolls up downstream. It is emphasized that the shear layer is self-exciting and no external forcing is used.

The experimental averaged streamlines (Fig. 14) exhibit a recirculating flow over the rear half-part of the flap, which is not reproduced by the present calculations (though the instantaneous snapshot shown in Fig. 13 presents a thin reverse flow region). This important discrepancy between experiment and zonal-DES is discussed further in the following paragraphs.

In Fig. 15, we focus on the wake of the main element and its development over the flap. The flow acceleration through the wing/flap gap is shown Fig. 15a. The velocity profile through the gap is slightly underpredicted by the RANS calculation but the wake width and deficit of the main airfoil is predicted fairly well by the zonal-DES. At the flap trailing edge, the experimental flow exhibits a separated boundary-layer profile. The extent of the computed region of reversed flow is thinner than experiment (Fig. 15b).

To investigate the flow through the gap, the velocity component fluctuations profiles for rake 4 are given Fig. 16. The rms fluctuation of the streamwise component of velocity is compared to the experiment in Fig. 16a. The highest levels near $d/c \approx 0.016$ are related to the small-scale vortex shedding occurring at the blunted trailing edge of the main element. The corresponding experimental peak value of $u_{\rm rms}/U_\infty \approx 17\%$ corroborates with earlier hot-wire measurements of Porcheron and Thibert[78] on the same profile. The second maximum near $d/c \approx 0.025$ is partly associated to the unsteadiness of boundary layer over the main element and to the wake of the slat. This second peak in underestimated by our zonal-DES approach because the upper side of the main element is explicitely treated in URANS mode.

Lower rms levels are encountered for the vertical velocity component (Fig. 16b) but the calculation overestimates the levels encountered in the trailing-edge wake of the main element.

The level of fluctuation of tranverse velocity component is given Fig. 16c. Minor differences are observed between the two grids on the maximum level of $w_{\rm rms}/U_\infty \approx 10\%$ occurring in wake. However, the effect of the spanwise grid extension Δ_z seems to be more important to evaluate the unsteadiness of the flow through the gap. Indeed, Fig. 12 revealed that the vortices that do escape through the gap are severely deformed by the accelerating local flow in such a way they become mainly longitudinal eddies. The spanwise grid extension Δ_z, therefore, has to be small enough to be able to capture these thin elongated eddies. Also note that the flow through the gap is unsteady and three-dimensional and that these features can not be reproduced by classical steady RANS calculations.

The TKE k_{uv} estimated using two components of the fluctuating flowfield is shown Fig. 16d. Similar comments to those for $u_{\rm rms}/U_\infty$ can be made. The kinetic energy peak is well predicted by zonal-DES, but the spreading of this peak is a bit too wide. This comes partly from the fact that the calculation is too dissipative.

Discussion

It has been observed experimentally that a separation occurs over the flap at about 50% of its chord lengthe[26] and a recirculation flow

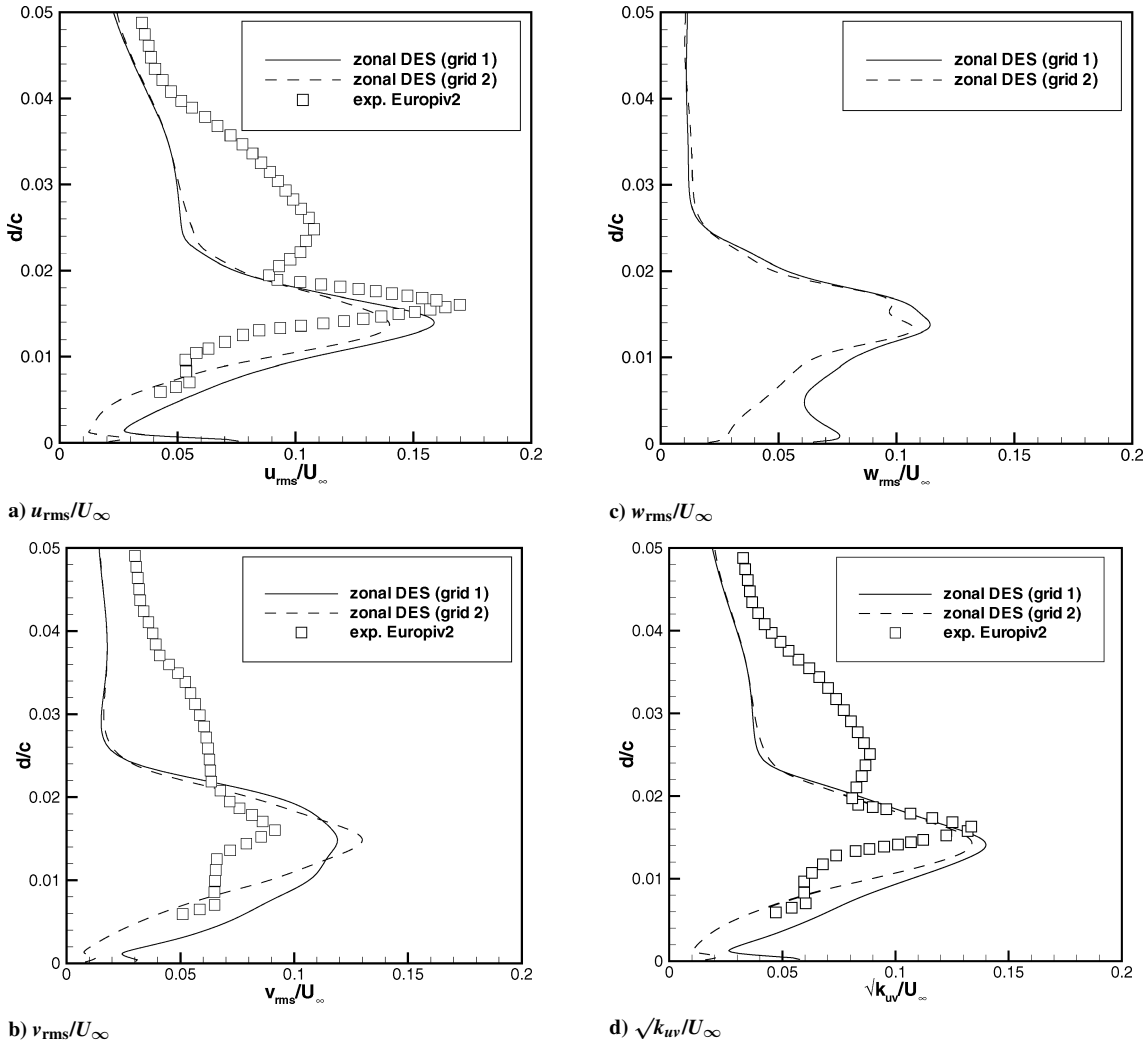

a) $u_{\mathrm{rms}}/U_\infty$ c) $w_{\mathrm{rms}}/U_\infty$

b) $v_{\mathrm{rms}}/U_\infty$ d) $\sqrt{k_{uv}}/U_\infty$

Fig. 16 Velocity fluctuations profiles (rake 4).

exists over the rear half of the flap. Nevertheless, it was found experimentally that separation and flow recirculation over the flap indeed occurred, although the phenomenon was intermittent. Arnott et al.[26] report two instantaneous PIV maps of the flow over the flap taken with a time interval of $\frac{2}{3}$ s. In the first, the high-velocity flow through the wing/flap gap remains fully attached over the flap, whereas in the second, a strong separation has occurred. It was found in this experiment[65] that over the flap the peak values of Cp are nearly independent from the angle of attack. No clear separation can be shown from the experimental pressure coefficient distribution (see Fig. 4). Cp distributions were not recorded during PIV measurement because the wing was covered with black foil to avoid reflections from the PIV laser, and this black foil covered the pressure holes.[26]

From the numerical side, Le Balleur and Neron[79] computed the same RA16SC1 HLD in similar conditions, for example, $\delta_{\mathrm{slat}} = 30$ deg, $\delta_{\mathrm{flap}} = -40$ deg, $Re_c = 1.8 \times 10^6$, and $\alpha = 16$ deg, to those used in this study with a viscous–inviscid solver associated to a two-equation turbulence model. They observed, depending on the initialization of the calculation, a realistic nonuniqueness of the separated flow solutions located either over the flap or in thick wake of the main element.

Also remember the work of Rumsey et al.,[80] who evaluated the effect of taking into account mounting hardware. In their study, brackets were included in unstructured-grid computation and were found to reduce the lift levels near maximum lift by 2–3%. In addition, deviations in the streamlines at high-lift conditions caused by the flap bracket as well as the boundary-layer development along the wind tunnel sidewalls can affect the two-dimensional character of the flap midspan flow. The authors concluded that faithful modeling of all surrounding walls and mounting hardware may be necessary.

These aspects and especially the explanation of the occurrence of separation over the flap need to be studied further in the future.

Conclusions

The numerical simulation of the unsteady flowfield around a whole high-lift element with deployed slat and flap is a problem of oustanding importance but is a very difficult and challenging case for DES because it presents thick boundary layers. Such a complex simulation has been possible thanks to the use of a zonal-DES method, allowing to reduce the cost of the simulation by limiting the extent of the DES zones while maintaining the desired level of accuracy in (U)RANS and focus regions. With this approach, the grid refinement is focused on regions of interest, for example, LES regions, without corrupting the boundary-layer properties farther upstream or downstream. Especially, the merging of the slat wake with the main body boundary layer is treated in RANS mode.

The effort is geared toward detailed validation of the flow in the slat and flap coves and downstream of the main element. Therefore, note that acquisition of experimental PIV data such as those performed in the EUROPIV2 project is of greatly help to validate hybrid RANS/LES methods and thus to improve the CFD methods that are used to design such high-lift systems. The statistical fields of velocity are generally well reproduced in the slat cove, including the mean velocity contours, the size of the recirculating bubble, as well as rms levels of the velocity fluctuations. Nevertheless, the levels of kinetic energy inside the separated area are underestimated.

Minor differences are observed on the mean field concerning the main element boundary layer between steady RANS and zonal-DES. The suction peak on the flap is not well reproduced by calculations, whereas the Cp value at the trailing edge compares favorably with experiment. Although no separation over the flap is clearly evidenced from the experimental pressure coefficient distribution, PIV data show a separated area over the flap that is recovered neither by RANS nor by zonal-DES. The occurrence of this separation remains unclear because Cp distributions were not recorded during PIV measurement. In an attempt to resolve this significant discrepancy, future work will focus on sidewall effects of the wind tunnel.

The present calculations provide an insight into the unsteady nature of the flow around a three-element airfoil that cannot be reproduced by classical steady RANS calculations. In the slat cove, important stages such as rollup and formation of discrete vortices are depicted. After experiencing severe distorsion at the reattachment point, some large and strong vortices are entrapped, whereas several vortices are ejected through the gap. Therefore, the slat wake inherits some structures from the cove, but they are highly stretched by the flow acceleration. Furthermore, the calculations revealed complex flow dynamics inside the flap cove. The separating shear layer from the flap cove lip rapidly becomes unstable, rolls up into large coherent vortices, and impinges the flap cove wall. Analogous to the slat region, the vortices that do escape through the gap are severely deformed by the accelerating local flow and mainly turned into longitudinal eddies. Therefore, the flow in the flap cove can influence the flow through the wing/flap gap, which in turn may affect the flow over the flap. The flow states are inherently related to one another, and the unsteady analysis of these flow features that are associated to aerodynamic noise emission will be a continuation of the present work.

Acknowledgments

The experimental work has been funded as part of the Europiv 2 program (EU Project G4RD-CT-2000-00190). In addition, the author thanks especially A. Schröder from DLR, German Aerospace Center, Institute of Aerodynamics and Flow Technology, and K. P. Neitzke from Airbus Germany for supplying the experimental data and for very stimulating e-mail exhanges. The DESider project (Detached Eddy Simulation for Industrial Aerodynamics) is a collaboration between Alenia, ANSYS-AEA, Chalmers University, Centre National de la Recherche–Lille, Dassault, DLR, EADS Military Aircraft, EUROCOPTER Germany, EDF, FOI-FFA, IMFT, Imperial College London, National Aerospace Laboratory, NTS, NUMECA, ONERA, TU Berlin, and UMIST. The project is funded by the European Community represented by the CEC, Research Directorate-General, in the 6th Framework Programme, under Contract AST-CT-2003-502842. The author is greatly indebted to his colleagues Pascal Thorigny for his valuable help in the mesh building process and Fréderic Moens for hours of fruitful discussion on high-lift aerodynamics.

References

[1]Woodward, D. S., and Lean, D. E., "Where Is High-Lift Today—A Review of Past UK Research Programs," *High-Lift System Aerodynamics*, CP-515, AGARD Sept. 1993, pp. 1.1–1.45.

[2]Thibert, J. J., Reneaux, J., Moens, F., and Priest, J., "ONERA Activities on High Lift Devices for Transport Aircraft," *Aeronautical Journal*, Vol. 99, No. 989, 1995, pp. 395–411.

[3]Ying, S. X., Spaid, F. W., McGinley, C. B., and Rumsey, C. L., "Investigation of Confluent Boundary Layers in High-Lift Flows," *Journal of Aircraft*, Vol. 36, No. 3, 1998, pp. 550–562.

[4]Rumsey, C. L., Gatski, T. B., Ying, S. X., and Bertelrud, A., "Prediction of High-Lift Flows Using Turbulent Closure Models," *AIAA Journal*, Vol. 36, No. 3, 1998, pp. 765–773.

[5]Catalano, P., and Amato, M., "An Evaluation of RANS Turbulence Modelling for Aerodynamic Applications," *Aerospace Science and Technology*, Vol. 7, Sept. 2003, pp. 493–509.

[6]Rudnik, R., Eliasson, P., and Peraud, J., "CFD Methods for Transport Aircraft High Lift Systems," Confederation of European Aerospace Societies Aerospace Aerodynamics, June 2002.

[7]Rudnik, R., "CFD Assesment for High lift Flows in the European Project EUROLIFT," AIAA Paper 2003-3794, June 2003.

[8]Hansen, H., Thiede, P., Rudnick, R., Moens, F., and Quest, J., "Overview About the European High Lift Research Program EUROLIFT," AIAA Paper 2004-0767, Jan. 2004.

[9]Khorrami, M. R., Singer, B. A., and Radeztsky, R. H., "Reynolds-Averaged Navier–Stokes Computations of a Flap-Side-Edge Flowfield," *AIAA Journal*, Vol. 37, No. 1, 1999, pp. 14–22.

[10]Mathias, D. L., Roth, K. R., Ross, J. C., Rogers, S. E., and Cummings, R. M., "Navier–Stokes Analysis of the Flow About a Flap Edge," *Journal of Aircraft*, Vol. 35, No. 6, 1999, pp. 833–838.

[11]Khorrami, M. R., Berkman, M. E., Li, F., and Singer, B. A., "Computational Simulations of a Three-Dimensional High-Lift Wing," AIAA Paper 2002-2804, June 2002.

[12]Jirasek, A., "A Vortex Generator Model and Its Application to Flow Control," AIAA Paper 2004-4965, Aug. 2004.

[13]van der Burg, J. W., Maseland, J. E. J., and Brandsma, F. J., "Low Speed Maximum Lift and Flow Control," *Aerospace Science and Technology*, Vol. 8, No. 5, 2004, pp. 389–400.

[14]Rogers, S. E., Roth, K., and Nash, S. M., "CFD Validation of High Lift Flows with Significant Wind Tunnel Effects," AIAA Paper 2000-4218, Aug. 2000.

[15]Melber-Wilkending, S., Wilhelm, R., and von Geyr, H. F., "RANS Solutions for a Complex High-Lift Configuration of a Transport Aircraft with Engine Including Improved Resolution of the Nearfield," AIAA Paper 2004-5081, Aug. 2004.

[16]Rumsey, C. L., and Ying, S. X., "Prediction of High Lift: Review of Present CFD Capability," *Progress in Aerospace Sciences*, Vol. 38, 2002, pp. 145–1801.

[17]Khorrami, M. R., Singer, B. A., and Lockard, D. P., "Time-Accurate Simulations and Acoustic Analysis of Slat Free-Shear Layer: Part II," AIAA Paper 2002-2579, 2002.

[18]Khorrami, M. R., Choudhari, M., Singer, B. A., Lockard, D. P., and Streett, C. L., "In Search of the Physics: The Interplay of Experiment and Computation in Slat Aeroacoustics," AIAA Paper 2003-0980, Jan. 2003.

[19]Khorrami, M. R., Berkman, M. E., and Choudhari, M., "Unsteady Flow Computations of a Slat with Blunt Trailing Edge," *AIAA Journal*, Vol. 38, No. 11, 2000, pp. 2050–2058.

[20]Terracol, M., Labourasse, E., Manoha, E., and Sagaut, P., "Simulation of the 3D Unsteady Flow in a Slat Cove for Noise Prediction," AIAA Paper 03-3110, 2003.

[21]Labourasse, E., and Sagaut, P., "Reconstruction of Turbulent Fluctuations Using a Hybrid RANS/LES Approach," *Journal of Computational Physics*, Vol. 182, 2002, pp. 301–336.

[22]Ben Khelil, S., "Large Eddy Simulation of Flow Around a Slat with a Blunt Trailing Edge," International Conf. on Computational Fluid Dynamics, July 2004.

[23]Roux, J. P., Guillen, P., Sagaut, P., Lirvat, J., Chen, H., Belanger, A., and Shock, R., "VLES of the Unsteady Flow Around a High Lift Wing Based on the Lattice Boltzmann Method," EuroMech Colloquium 449 Computational AeroAcoustics: From Acoustic Sources Modeling to Far-Field Radiated Noise Prediction, Euromech, Dec. 2003.

[24]Stanislas, M., Kompenhans, J., and Westerweel. J. (eds.), *Particle Image Velocimetry—Progress Towards Industrial Applications*, Kluwer, Dordrecht, The Netherlands, 2000.

[25]Spalart, P. R., and Bogue, D. R., "The Role of CFD in Aerodynamics, Off-Design," *Aeronautical Journal*, Vol. 107, No. 1072, 2003, pp. 323–330.

[26]Arnott, A., Neitzke, K. P., Agocs, J., Sammer, G., Schneider, G., and Schroeder, A., "Detailed Characterisation Using PIV of the Flow Around an Aerofoil in High Lift Configuration," *EUROPIV2 Workshop on Particle Image Velocimetry*, Springer, Berlin, 2003.

[27]Mary, I., and Sagaut, P., "Large Eddy Simulation of Flow Around an Airfoil near Stall," *AIAA Journal*, Vol. 40, No. 6, 2002, pp. 1139–1145.

[28]Péchier, M., "Prévisions numériques de l'Effet Magnus pour des Configurations de Munition," Ph.D. Dissertation, Dept. of Mechanical Engineering, Univ. de Poitiers, Poitiers, France, Sept. 1999.

[29]Péchier, M., Guillen, P., and Caysac, R., "Magnus Effect over Finned Projectiles," *Journal of Spacecraft and Rockets*, Vol. 38, No. 4, 2001, pp. 542–549.

[30]Deck, S., Duveau, P., d'Espiney, P., and Guillen, P., "Development and Application of Spalart Allmaras One Equation Turbulence Model to Three-Dimensional Supersonic Complex Configurations," *Aerospace Science and Technology*, Vol. 6, No. 3, 2002, pp. 171–183.

[31]Raverdy, B., Mary, I., Sagaut, P., and Liamis, N., "High-Resolution Large-Eddy Simulation of the Flow Around a Low Pressure Turbine Blade," *AIAA Journal*, Vol. 41, No. 3, 2003, pp. 390–397.

[32]Larchevêque, L., Labbé, O., Mary, I., and Sagaut, P., "LES of a Compressible Flow past a Deep Cavity," *Physics of Fluids*, Vol. 15, No. 1, 2003, pp. 193–210.

[33]Deck, S., "Detached Eddy Simulation of Transonic Buffet over a Supercritical Airfoil," AIAA Paper 2004-5378, Aug. 2004.

[34]Travin, A., Shur, M., Spalart, P., and Strelets, M., "On URANS Solutions with LES-like Behavior," *ECCOMAS, Proceedings European Congress on Computational Methods in Applied Sciences and Engineering*, edited by P. Neittaanmäki, T. Rossi, K. Majava, and O. Pironneau, July 2004.

[35]Spalart, P., Jou, W. H., Strelets, M., and Allmaras, S. R., "Comments on the Feasibility of LES for Wings and on a Hybrid RANS/LES Approach," *1st AFSOR Int. Conf. on DNS/LES*, Greyden Press, Columbus, OH, 1997, pp. 137–147.

[36]Speziale, C. G., "Turbulence Modeling for Time-Dependent RANS and VLES: A Review," *AIAA Journal*, Vol. 36, No. 2, 1998, pp. 173–184.

[37]Batten, P., Goldberg, U., and Chakravarthy, S., "LNS—An Approach Towards Embedded LES," AIAA Paper 2002-0427, Jan. 2002.

[38]Menter, F. R., Kuntz, M., and Bender, R., "A Scale-Adaptive Simulation Model for Turbulent Flow Predictions," AIAA Paper 2003-0767, Jan. 2003.

[39]Kok, J. C., Dol, H. S., Oskam, H., and van der Ven, H., "Extra-Large Eddy Simulation of Massively Separated Flows," AIAA Paper 2004-0264, Jan. 2004.

[40]Baurle, R. A., Tam, C. J., Edwards, J. R., and Hassan, H. A., "Hybrid Simulation Approach for Cavity Flows: Blending, Algorithm, and Boundary Treatment Issues," *AIAA Journal*, Vol. 41, No. 8, 2003, pp. 1463–1480.

[41]Spalart, P. R., "Strategies for Turbulence Modelling and Simulations," *International Journal of Heat and Fluid Flows*, Vol. 21, No. 3, 2000, pp. 252–263.

[42]Strelets, M., "Detached Eddy Simulation of Massively Separated Flows," AIAA Paper 2001-0879, Jan. 2001.

[43]Squires, K. D., Forsythe, J. R., Morton, S. A., Strang, W. Z., Wurtzler, K. E., Tomaro, R. F., Grismer, M. J., and Spalart, P. R., "Progress on Detached-Eddy Simulation of Massively Separated Flows," AIAA Paper 2002-1021, Jan. 2002.

[44]Forsythe, J. R., Squires, K. D., Wurtzler, K. E., and Spalart, P. R., "Detached-Eddy Simulation of Fighter Aircraft at High Alpha," *Journal of Aircraft*, Vol. 41, No. 2, 2004, pp. 193–200.

[45]Deck, S., Garnier, E., and Guillen, P., "Turbulence Modelling Applied to Space Launcher Configurations," *Journal of Turbulence*, Vol. 3, No. 57, 2002, pp. 1–21.

[46]Morton, S. A., Cummings, R. M., and Kholodar, D. B., "High Resolution Turbulence Treatment of F/A-18 Tail Buffet," AIAA Paper 2004-1676, April 2004.

[47]Spalart, P. R., "Topics in Detached Eddy Simulation," International Conf. on Computational Fluid Dynamics, July 2004.

[48]Squires, K. D., "Detached-Eddy Simulation: Current Status and Perspectives," *Proceedings of Direct and Large-Eddy Simulation-5*, Kluwer, Dordrecht, The Netherlands, pp. 465–480.

[49]Spalart, P. R., and Allmaras, S. R., "A One Equation Turbulence Model for Aerodynamic Flows," AIAA Paper 92-0439, 1992.

[50]Spalart, P. R., and Allmaras, S. R., "A one Equation Turbulence Model for Aerodynamic Flows," *La Recherche Aérospatiale*, Vol. 1, Jan. 1994, pp. 5–21.

[51]Spalart, P., "Trends in Turbulence Treatments," AIAA Paper 2000-2306, 2000.

[52]Nikitin, N. V., Nicoud, F., Wasistho, B., Squires, K. D., and Spalart, P. R., "An Approach to Wall Modeling in Large Eddy Simulation," *Physics of Fluids*, Vol. 12, July 2000, pp. 1629–1631.

[53]Piomelli, U., Balaras, E., Squires, K. D., and Spalart, P. R., "Interaction of the Inner and Outer Layers in Large Eddy Simulations with Wall-Layer Models," *International Journal of Heat and Fluid Flows*, Vol. 24, 2003, pp. 538–550.

[54]Caruelle, B., and Ducros, F., "Detached-Eddy Simulation of Attached and Detached Boundary Layers," *International Journal of Computational Fluid Dynamics*, Vol. 17, No. 6, 2003, pp. 433–451.

[55]Forsythe, J. R., Fremaux, C. M., and Hall, R. H., "Calculation of Static and Dynamic Stability Derivatives of the F/A-18E in Abrupt Wing Stall Using RANS and DES," International Conf. on Computational Fluid Dynamics, July 2004.

[56]Spalart, P. R., Deck, S., Shur, M. L., Squires, K. D., Strelets, M., and Travin, A., "A New Version of Detached-Eddy Simulation, Resistant to Grid Ambiguous Grid Densities," *Theoretical and Computational Fluid Dynamics* (submitted for publication).

[57]Spalart, P. R., "Young-Person's Guide to Detached Eddy Simulation Grids," NASA Technical Rept. CR-2001-211032, July 2001.

[58]Deck, S., "Numerical Simulation of Transonic Buffet over a Supercritical Airfoil," *AIAA Journal*, Vol. 43, No. 7, 2005, pp. 1556–1566.

[59]Batten, P., Goldberg, U., and Chakravarthy, S., "Interfacing Statistical Turbulence Closures with Large-Eddy-Simulation," *AIAA Journal*, Vol. 42, No. 3, 2004, pp. 485–492.

[60]Schluter, J. U., Pitsch, H., and Moin, P., "Large Eddy Simulation Inflow Conditions for Coupling with Reynolds-Averaged Flow Solvers," *AIAA Journal*, Vol. 42, No. 3, 2004, pp. 478–484.

[61]Sagaut, P., Garnier, E., Tromeur, E., Larcheveque, L., and Labourasse, E., "Turbulent Inflow Conditions for Large-Eddy-Simulation of Compressible Wall-Bounded Flows," *AIAA Journal*, Vol. 42, No. 3, 2004, pp. 469–477.

[62]Breuer, M., Jovicic, N., and Mazaev, K., "Comparison of DES, RANS and LES for the Separated Flow Around a Flat Plate at High Incidence," *International Journal for Numerical Methods in Fluids*, Vol. 41, 2003, pp. 357–388.

[63]Guénot, D., "Simulations des Effets instationnaires á grande Échelle dans les Écoulements décollés," Ph.D. Dissertation, Fluid Mechanics Dept., Ecole Nationale Supérieure de l'Aéronautique et de l'Espace, Toulouse, France, 2004.

[64]Shur, M., Spalart, P. R., Strelets, M., and Travin, A., "Modification of SA Subgrid Model in DES Aimed to Prevent Activation of the Low-RE Terms in LES Mode," DES Workshop, St. Petersburg, Russia, July 2003.

[65]Neitzke, K. P., "Using Advanced Measurement Techniques in High Lift Validation Experiments," Royal Aerospace Society, Aerospace Aerodynamics Research Conf. June 2003.

[66]Paterson, E. G., and Peltier, L. J., "Detached-Eddy Simulation of High-Reynolds Number Beveled-Trailing-Edge Flows and Wakes," American Society of Mechanical Engineers Heat Transfer/Fluids Engineering Summer Conf., Symposium on Advancement and Applications of LES, July 2004.

[67]Paterson, E. G., and Baker, W. J., "RANS and Detached-Eddy Simulation of the NCCR Airfoil," NASA–ONR Circulation Control Workshop, March 2004.

[68]Khorrami, M. R., Choudhari, M. M., and Jenkins, L. N., "Characterization of Unsteady Flow Structures Near Leading-Edge Slat: Part II. 2D Computations," AIAA Paper 2004-2802, 2004.

[69]Moens, F., "EUROLIFT-ST.2.1.1: Assessment of CFD Methods for High-Lift Applications. ONERA RANS 2D activity," ONERA, Rept. 75/03631, Oct. 2001.

[70]Moens, F., "GARTEUR Aerodynamics AG25. CFD Prediction of Maximum Lift of a 2D High Lift Configuration," Katnet/GARTEUR Highlift Workshop, Paper 44, Sept. 2002.

[71]Dillner, B., May, F. W., and Mc Masters, J. H., "Aerodynamics Issues in the Design of Highlift Systems for Transport Aircraft," CP365, AGARD, Paper 9, May 1984.

[72]Seraudie, A., Perraud, J., and Moens, F., "Transition Measurement and Analysis on a Swept Wing in High Lift Configuration," *Aerospace Science and Technology*, Vol. 7, No. 8, 2003, pp. 569–576.

[73]Delcayre, F., and Dubief, Y., "On Coherent-Vortex Identification in Turbulence," *Journal of Turbulence*, Vol. 1, No. 11, 2000, pp. 1–22.

[74]Takeda, K., Ashcrott, G. B., Zhang, X., and Nelson, P. A., "Unsteady Aerodynamics of Slat Cove Flow in a High-Lift Device Configuration," AIAA Paper 2001-0706, Jan. 2001.

[75]Paschal, K., Jenkins, L., and Yao, C., "Unsteady Slat-Wake Characteristics of a High-Lift Configuration," AIAA Paper 2000-0139, Jan. 2000.

[76]Jenkins, L. N., Khorrami, M. R., and Choudhari, M. M., "Characterization of Unsteady Flow Structures near Leading-Edge Slat: Part I. PIV Measurements," AIAA Paper 2004-2802, 2004.

[77]Takeda, K., Ashcrott, G. B., Zhang, X., and Nelson, P. A., "Unsteady Aerodynamics of Flap Cove Flow in a High-Lift Device Configuration," AIAA Paper 2001-0707, Jan. 2001.

[78]Porcheron, B., and Thibert, J. J., "Etude détaillée de l'Écoulement autour d'un Profil hypersustenté. Comparaisons avec les Calculs," AGARD Symposium on Improvement of Aerodynamics Performance Through Boundary Layer Control and High-Lift System, ONERA TP 1984-17, May 1984.

[79]Le Balleur, J. C., and Neron, M., "A Viscous–Inviscid Solver for High Lift Incompressible Flows over Multi-Element Airfoils at Deep Separation Conditions," CP-515, AGARD, Sept. 1993, pp. 11.1–11.12.

[80]Rumsey, C. L., Lee-Rausch, E. M., and Watson, R. D., "Three-Dimensional Effects on Multi-Element High Lift Computation," AIAA Paper 2002-0845, Jan. 2002.

R. So
Associate Editor